



1 **Application of regional meteorology and air quality models**
2 **based on MIPS CPU Platform**

3

4 **Zehua Bai^{1,2}, Qizhong Wu^{1,2}, Kai Cao^{1,2}, Yiming Sun³, Huaqiong Cheng^{1,2}**

5

6 ¹College of Global Change and Earth System Science, Faculty of Geographical Science,
7 Beijing Normal University, Beijing 100875, China.

8 ²Joint Center for Earth System Modeling and High Performance Computing, Beijing
9 Normal University, Beijing 100875, China.

10 ³Beijing Institute of Talent Development Strategy, Beijing 100032, China.

11

12 **Correspondence:** Qizhong Wu (wqizhong@bnu.edu.cn)

13

14 **Abstract.** The MIPS processor architecture is a type of Reduced Instruction Set
15 Computing (RISC) processor architecture, which has advantages in terms of energy
16 consumption and efficiency. There are few studies on the application of MIPS CPUs in
17 the geoscientific numerical models. In this study, Loongson 3A4000 CPU platform with
18 MIPS64 architecture was used to establish the runtime environment for the air quality
19 modelling system WRF-CAMx in Beijing-Tianjin-Hebei region. The results show that
20 the relative errors for the major species (NO₂, SO₂, O₃, CO, PNO₃ and PSO₄) between
21 the MIPS and X86 benchmark platform are within ±0.1%. The maximum Mean
22 Absolute Error (MAE) of major species ranged to 10⁻² ppbV or µg m⁻³, the maximum
23 Root Mean Square Error (RMSE) ranged to 10⁻¹ ppbV or µg m⁻³, and the Mean Absolute
24 Percentage Error (MAPE) remained within 0.5%. The CAMx takes about 15.2 minutes
25 on Loongson 3A4000 CPU and 4.8 minutes on Intel Xeon E5-2697 v4 CPU, when
26 simulating a 2h-case with four parallel processes using MPICH. As a result, the single-
27 core computing capability of Loongson 3A4000 CPU for the WRF-CAMx modeling
28 system is about one-third of Intel Xeon E5-2697 v4 CPU, but the thermal design power
29 (TDP) of Loongson 3A4000 is 30W, only about one-fifth of Intel Xeon E5-2697 v4,



30 which TDP is 145W. Thus, Loongson 3A4000 has higher energy efficiency in the
31 application of the WRF-CAMx modeling system. The results also verify the feasibility
32 of cross-platform porting and the scientific usability of the ported model. This study
33 provides a technical foundation for the porting and optimization of numerical models
34 based on MIPS or other RISC platforms.

35

36 **1 Introduction**

37 In the recent years, with the increasing demand for high-performance computing
38 resources and rapid development in the computer industry, especially supercomputer,
39 central processing unit (CPU) has undergone significant advancements in logical
40 structure, operational efficiency, and functional capabilities, making it the core
41 component of current computer technology development. There are two main types:
42 one is complex instruction set computer (CISC) CPU (George, 1990; Shi, 2008), mainly
43 using X86 architecture, representative vendors including Intel, AMD, etc., and widely
44 used in high-performance computing platforms. The other is reduced instruction set
45 computer (RISC) CPU (Mallach, 1991; Liu et al., 2022), mainly using ARM, MIPS,
46 RISC-V and other architectures, representative vendors including Loongson, etc., and
47 mainly used in high-performance computing platforms, which have high efficiency,
48 excellent stability and scalability. The Microprocessor without interlocked piped stages
49 (MIPS) architecture is one of the significant representatives of RISC architecture. MIPS
50 was originally developed in the early 1980s by Professor Hennessy at Stanford
51 University and his group (Hennessy et al., 1982). The simplicity of the MIPS instruction
52 set contributes to its ability to process instructions quickly, thus achieving higher
53 performance even in low-power conditions. In 1999, MIPS Technology Inc. released
54 the MIPS32 and MIPS64 architecture standard (MIPS Technology Inc., 2014).
55 Compared to the CISC CPUs, RISC CPUs demonstrate excellent performance and
56 power efficiency, which have gained popularity among chip manufacturers.

57 The Loongson processor family developed by Loongson Technology is mainly
58 designed using MIPS architecture and Linux operating system (Hu et al, 2011), which



59 has rich application tools in Linux open-source projects. The main reason that currently
60 restricts the development of CPUs that implement non-X86 instruction set architecture
61 such as MIPS64 is the immature software ecosystem (Hu et al., 2016). Based on the
62 strategy of open-source software, Loongson platform has gained abundant software
63 tools, making it possible to further develop scientific computing and numerical models.

64 Air quality model (AQM) systems use mathematical equations and algorithms to
65 simulate and predict the pollutant concentration in the atmosphere. The current AQMs
66 have become more complex, incorporating numerous factors such as emissions from
67 industrial sources, vehicle traffic, and natural sources, as well as meteorological
68 conditions, including modeling meteorology, emissions, chemical reactions, and
69 removal processes (Zhang et al., 2012). Regional-scale AQMs have been widely used
70 to predict air quality in cities, formulate emission reduction strategies, and evaluate the
71 effectiveness of control polices (Wang et al., 2023), including the Community
72 Multiscale Air Quality (CMAQ) modelling system (Appel et al., 2017; Appel et al.,
73 2021), the Comprehensive Air Quality Model with extensions (CAMx; RAMBOLL
74 ENVIRON Inc., 2014), and the Nested Air Quality Prediction Modeling System (Wang
75 et al., 2006; Chen et al., 2015). Due to the requirement of meteorological input,
76 commonly used offline meteorological models such as WRF (Michalakes et al., 2001)
77 are coupled offline with the regional AQMs to provide meteorological and chemical
78 forecast as the WRF-AQM modeling system, such the WRF-CMAQ modeling system
79 (Wu et al., 2014).

80 Both the meteorological and air quality numerical simulation rely heavily on high-
81 performance computing systems. The WRF-AQM systems can run stably on high-
82 performance computing platforms based on X86 or X86-compatible instruction set
83 architecture (ISA) CPUs, which account for the highest percentage among the main
84 processors of current high performance computing platforms. There are relatively
85 limited researches on the application of WRF-AQM system on MIPS CPU platforms at
86 present, this study focuses on the application of WRF-CAMx model on Loongson CPU
87 platform based on the MIPS architecture. A simulation case covering the Beijing-
88 Tianjin-Hebei region was set up to evaluate the differences and performance between



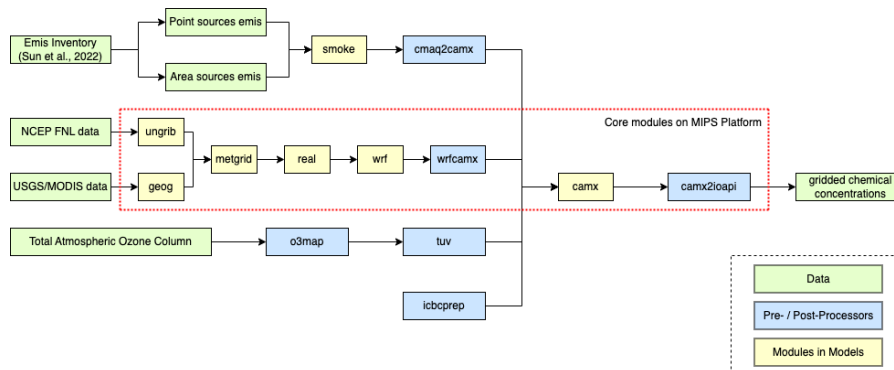
89 MIPS and X86 platforms. This study validated the stability of scientific computing on
 90 MIPS CPU platform, and it offered technical references and evaluation methods for the
 91 porting and application of numerical models on non-X86 platforms.

92 The remainder is organized as follows. Section 2 provides the model descriptions
 93 of the Weather Research and Forecasting–Comprehensive Air Quality Model with
 94 extensions (WRF-CAMx) modeling system, and the platform descriptions of both
 95 MIPS CPU platform and benchmark platform. The configuration of the air quality
 96 numerical simulation system and simulation case are also presented in Section 2.
 97 Section 3 describes porting and optimization of the WRF-CAMx modelling system on
 98 MIPS CPU platform. Section 4 analyzes the differences of model results between MIPS
 99 CPU platform and the benchmark platform. Section 5 discusses MIPS CPU
 100 performance in scientific computing. The conclusions are presented in Section 6.

101

102 2 Model and Porting Platform Description

103 The air quality modeling system was constructed using the WRF v4.0 model
 104 developed by National Center for Atmospheric Research (NCAR) (Skamarock et al.,
 105 2019), and the CAMx v6.10 developed by Ramboll Environment (RAMBOLL
 106 ENVIRON Inc., 2014), as shown in Figure 1. And the Loongson 3A4000 CPU platform
 107 was chosen for the porting work in the study. This study introduced the porting of WRF-
 108 CAMx modeling system to MIPS CPU platform.



109

110 **Figure 1.** Framework of WRF-CAMx modeling system. The core modules have been
 111 ported to MIPS CPU platform. The core modules are framed by red dashed line in the



112 figure.

113 In Xi'an, China and Milan, Europe, the WRF-CAMx modelling system was
114 developed, enabling high-resolution hourly model output of pollutant concentration
115 within specific local urban areas (Pepe et al., 2016; Yang et al., 2020). The modeling
116 system is widely used to study the spatial-temporal variation of pollutant concentration
117 and source apportionment, analyze the contribution of regional transport to pollution
118 and investigate the impact of initial conditions and emissions on pollution simulation
119 in key regions such as the North China Plain, Sichuan Basin, and Fenwei Plain (Bai et
120 al., 2021; Zhen et al., 2023; Zhang et al., 2022; Xiao et al., 2021).

121

122 **2.1 Description of WRF-CAMx modeling system**

123 WRF and CAMx serve as the core components of the modeling system. WRF is a
124 high-resolution mesoscale model, which can be utilized for various purposes such as
125 weather research and forecasting, physical parameterization scheme research, data
126 assimilation and mesoscale climate simulation. In the modeling system, WRF provided
127 gridded meteorological field data for air quality model CAMx. CAMx is an atmospheric
128 pollutant calculation model, which can be utilized for simulating and predicting the
129 concentrations of various air pollutants. The WRF and CAMx models are distinguished
130 by modularity and parallelism, using MPI in parallel computing, making them efficient
131 (Skamarock et al., 2019; RAMBOLL ENVIRON Inc., 2014).

132 In the modeling system, the SMOKE model and cmaq2camx program are used to
133 process emission data and provide model-ready gridded emission data for the CAMx
134 model. The wrfcamx program converts the WRF results into meteorological input files
135 which are compatible with CAMx. TUV is a radiation transfer model capable of
136 producing clean sky photolysis rate input files for the chemical mechanisms in CAMx,
137 and the o3map program prepares ozone column input files for TUV and CAMx. The
138 icbcprep program prepares initial and boundary condition files for CAMx with the
139 profile, and the effects of initial conditions have been studied by Xiao et al. (2021). The
140 camx2ioapi program converts the CAMx output files into netCDF format following the
141 Models-3/IO-API convention, and then uses NCL or other softwares to analyses the

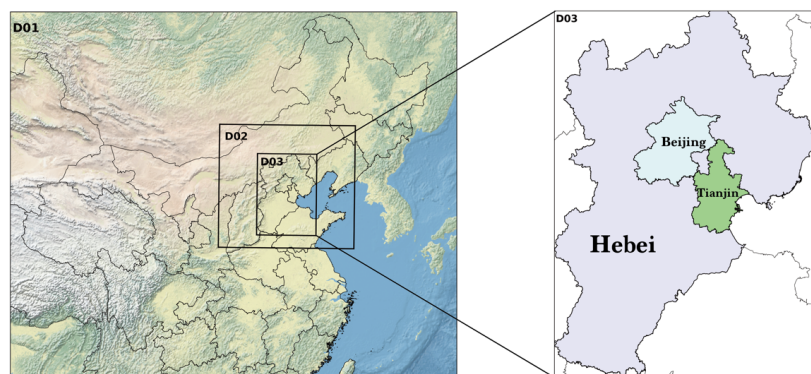


142 model results.

143

144 **2.1.1 Model domain setup**

145 The model domain focusing on the Beijing-Tianjin-Hebei region has been set up
146 in this study. The WRF model has three nested domains with horizontal resolutions of
147 27km (D1), 9km (D2), and 3km (D3), as shown in Figure 2. The outer domain (D1)
148 covers most parts of China, and the inner domain (D3) covers Beijing, Tianjin, and
149 Hebei Province. The model domain is centered at (35°N, 110°E), with two true latitudes
150 located at 20°N and 50°N. The vertical resolution of WRF is 34 vertical layers. The
151 CAMx model has only one model domain, which is the innermost grid with a resolution
152 of 3km (D3), mainly covering the Beijing-Tianjin-Hebei region. The vertical resolution
153 of CAMx is 14 vertical layers, which is extracted from the WRF output files using the
154 wrfcamx module, and the lower seven layers of CAMx are same as those in the WRF
155 model.



156

157 **Figure 2.** The domains of three-level nested grids in the WRF-CAMx modelling system.

158 The respective horizontal resolutions are 27 km × 27 km (D1), 9 km × 9 km (D2), and
159 3 km × 3 km (D3).

160

161 **2.1.2 Model configuration**

162 For the meteorological model, the global meteorological initial and boundary
163 fields for the WRF model are derived from the NCEP Global Final Reanalysis Data



164 (FNL), with a spatial resolution of $0.5^\circ \times 0.5^\circ$ and a temporal resolution of 6 hours. And
165 the parameterization schemes of the WRF model used in the simulation case are shown
166 in Table 1.

167 For the air quality model, the meteorological files are provided by the WRF model
168 are used for the chemical transport module in CAMx. The emission inventory used in
169 the simulation case was obtained from Sun et al. (2022a). It contains basic emissions
170 from Sun et al. (2022b) and fugitive dust emission from bare ground surfaces. The
171 SMOKE model (v2.4) is used to process the emission inventory and provide gridded
172 emissions for CAMx. The parameterization schemes of the CAMx model used in the
173 simulation case are shown in Table 2.

174

175 **Table 1.** Parameterization schemes of WRF in research case.

Parameterization process	Scheme
Microphysics	WSM3
Longwave radiation	RRTM
Shortwave radiation	Dudhia
Land surface	Noah
Planetary boundary layer	YSU
Cumulus parameterization	Kain-Fritsch(new Eta)

176

177 **Table 2.** Parameterization schemes of CAMx in research case.

Parameterization process	Scheme
Horizontal Diffusion	PPM
Vertical Diffusion	K-theory
Dry Deposition	Zhang03
Gas-phase chemical mechanism	CB05
Aqueous aerosol chemistry	RADM-AQ
Inorganic gas-aerosol partitioning	ISORROPIA

178

179 2.2 MIPS CPU platform description

180 Loongson CPU platform was chosen for the porting work in the study. Currently,
181 the Loongson processor family has three generations of CPU products, evolving from
182 single-core to multi-cores architectures and from experimental prototypes to mass-
183 produced industrial products (Hu et al., 2011). The Loongson-2 processor is a 64-bit



184 general-purpose RISC processor series which is compatible with MIPS instruction set.
185 It can be used in personal computers, mobile terminals, and various embedded
186 applications, running many operating systems such as Linux and Android smoothly
187 (Zhi et al., 2012). Wu et al. (2019) reports the application of the mesoscale model on
188 Loongson 2F CPU platform. The Loongson-3 processor features a scalable multi-core
189 architecture, targeting high-throughput data centers, high-performance scientific
190 computing, and other applications, with the significant advantage of achieving a high
191 peak performance-to-power ratio and striking a well-balanced trade-off between
192 performance and power consumption (Hu et al., 2009).

193 A lot of porting and optimization research work has been conducted to ensure the
194 proper functioning of the high-performance mathematical library on Loongson
195 platforms, resulting in improved computing performance, such as FFT (Fast Fourier
196 Transform) (Guo et al., 2012; Li et al., 2011; Zhao et al., 2012). The porting and
197 optimization efforts conducted on the multi-core Loongson processors have
198 successfully demonstrated the stability and efficiency in the numerical computing
199 applications. These results provide valuable technical references and rationality
200 validation for the numerical model application on Loongson platform.

201 The Loongson 3A series are multi-core processors designed for high-performance
202 computers, featuring with high bandwidth, and low power consumption. The efficient
203 design solution and the advantage of high energy efficiency ratio make servers based
204 on Loongson CPUs highly competitive in performance, power consumption, and cost-
205 effectiveness (Li et al., 2014; Wang et al., 2014). In this study, the Loongson platform
206 uses the Debian Linux operating system, commercially known as Tongxin UOS
207 (<https://www.uniontech.com>, last access: October 2023), and the Loongson 3A4000
208 processor, which is the first quad-core processor based on GS464v 64-bit
209 microarchitecture in Loongson 3 Processor Family. The main technical parameters of
210 Loongson 3A4000 CPU are shown in Table 3. Compared to previously released CPUs,
211 the processor improves frequency and performance by optimizing on-chip interconnect
212 and memory access path, integrating 64-bit DDR4 memory controller and on-chip
213 security mechanism.



214

215 **Table 3.** Main Parameters of Loongson 3A4000 CPU*

Loongson 3A4000 CPU Main Parameters	
Main Frequency	1.8GHz–2.0GHz
Peak Computing Speed	128GFlops@2.0GHz
Transistor Technology	28nm
Number of Cores	4
Processor Cores	MIPS64 compatible Support 128/256-bit vector instructions
High-speed I/O	2 x 16-bit HyperTransport 3.0 control
Typical Power Consumption	<30W@1.5GHz
	<40W@1.8GHz
	<50W@2.0GHz

216 *source: <https://www.loongson.cn>, last access: October 2023.

217

218 **2.3 Benchmark platform description**

219 This study uses an X86 CPU platform as benchmark platform compared to the
 220 MIPS CPU platform. The benchmark platform is powered by Intel Xeon E5-2697 v4
 221 CPU, with strong floating-point performance and many technical features such as Intel
 222 Turbo Boost Technology (Intel Inc., 2023). The Intel Xeon E5-2697 v4 CPU has 18
 223 cores, with 2.3GHz base frequency and 3.6GHz maximum Turbo Boost frequency, 45
 224 MB Intel Smart Cache and 145W design power consumption. The operating system is
 225 CentOS Linux 7.4.1708. The main information for both platforms is shown in Table 4.

226

227 **Table 4.** The comparison of main configuration between MIPS and X86 platforms.

	MIPS Platform	X86 platform
CPU	Loongson 3A4000	Intel Xeon E5-2697 v4
Number of CPUs	1	1
Number of CPU cores	4	18
CPU Frequency	1.8GHz	2.3GHz
CPU instruction set	MIPS64	X86_64
Operating system	Tongxin UOS	CentOS Linux 7.4.1708
Operating system kernel (Linux version)	4.19.0-loongson-3-desktop	3.10.0-957.1.3.el7.x86_64

228

229 **2.4 The difference between MIPS and X86 platforms**



230 In this study, the numerical model’s source code is written in Fortran, and
 231 commonly used compilers for X86 architecture include Intel Compiler, PGI and GNU
 232 Compiler. The compiler for MIPS platform is built using GCC 8.3 MIPS GNU/Linux
 233 cross-toolchain based on the open-source GNU Project, called MIPS GNU, and the
 234 latest version is 8.3. The compiler for the benchmark platform is set to X86 GNU, and
 235 the version is also 8.3. Table 5 shows the differences between the two platforms' GNU
 236 compilers in terms of applicable platforms. Compared to X86 GNU, the default
 237 compilation options of MIPS GNU compiler not only specify the platform architecture
 238 but also include additional instruction sets, such as atomic operation instruction set
 239 LLSC, shared library instruction set PLT, etc., which can optimize target programs
 240 compiled by GNU for MIPS architecture and improve computational efficiency.

241 **Table 5.** Comparison of GNU compiler between MIPS and X86 CPU platforms.

Artitecture	MIPS64	x86_64
Compiler	MIPS GNU Fortran	X86 GNU Fortran
Version	8.3	8.3
Target	mips64el-linux-gnuabi64	x86_64-redhat-linux
Options	-march=mips64r2	-march=x86-64
(Architecture)	-mabi=64	-mtune=generic
Options	-mllsc -mplt -mmadd4	/
(Instruction set)		
FLAGS(WRF)	-fconvert=big-endian -frecord-marker=4 -ffree-line-length-none -O2 -ftree-vectorize -funroll-loops	
FLAGS(CAMx)	-fconvert=big-endian -frecord-marker=4 -ffixed-line-length-none -fno-align-commons -O2	

242 The WRF-CAMx modeling system depends on several scientific computing
 243 libraries. Firstly, the general data format libraries netCDF and HDF5 are required to
 244 store the large-scale gridded data for the modeling system. NetCDF is a self-describing
 245 data format developed by NCAR/Unidata, primarily used for storing multidimensional
 246 array data in fields like meteorology and earth sciences (UCAR/Unidata, 2021). HDF5
 247 is a data format developed by HDF GROUP that supports complex data structures with
 248 multiple data types and multi-dimensional datasets (The HDF Group, 2019). In this
 249 study, netCDF-C (v4.8.1), netCDF-Fortran (v4.5.3), HDF5 (v1.12.1) and IOAPI (v3.1)
 250 were successfully installed on MIPS platform by building from their sources, which are



251 obtained from the official website.

252 The MPICH library is required to support parallel computing in the modeling
253 system. In order to fully utilize computing resources, the method of MPI message
254 communication is used in WRF and CAMx model (Wu et al., 2012). MPICH is an
255 open-source, portable parallel computing library for implementing the MPI standard
256 (Amer et al., 2021). It supports inter-process communication and data exchange in the
257 parallel computing environment. Similarly, this study successfully installed MPICH
258 (v3.4) on MIPS platform by building from its source. During the compilation and
259 installation of the mentioned libraries above, the configure tool was used to check the
260 basic information of the platform's CPU and compiler, and prepare for compatibility
261 with platform before compilation, the GNU compiler is used to compile the source code
262 of libraries, and the cmake tool is used to install the libraries. Additionally, the same
263 runtime environment as MIPS platform was also built on the benchmark platform.

264

265 **3 Porting the WRF-CAMx modelling system on MIPS CPU platform**

266 The simulation result is influenced by several factors including processor
267 architecture, operating system, compiler, parallel environment, and scientific
268 computing libraries. In order to ensure stability and accuracy of numerical simulation,
269 the models should be adapted to the new runtime environment when porting across
270 platforms. Additionally, various operating systems have different tools, software and
271 libraries, which may impact the results of numerical simulations.

272 In this study, the runtime environment for WRF-CAMx modeling system was built
273 on MIPS platform. The configuration files for making the models were modified to fit
274 the compiler of the UOS Linux system on MIPS platform. In order to verify the stability
275 of scientific computing on MIPS platform, a control experiment was set up on the
276 benchmark platform, minimizing the impact of other factors on simulation results of
277 both platforms.

278 The WRF v4.0 and CAMx v6.10 were successfully deployed on MIPS platform
279 through source code compilation and installation. In the WRF model, the default



280 options for GNU compiler which are suitable for MIPS architecture CPU are not
281 provided in the configure file of the source code package, and it is necessary to
282 manually add information about the CPU architecture, GNU compiler, and compilation
283 flags on MIPS platform. Table 5 provides the detailed information added in the
284 configure file, mainly about MIPS GNU Fortran. When compiling Fortran programs on
285 MIPS platform, the MIPS GNU Fortran and necessary compilation flags must be
286 specified. These flags include common Fortran file format flags such as `-fconvert=big-`
287 `endian` and `-frecord-marker=4`, as well as optimization flags such as `-O2` `-ftree-`
288 `vectorize` `-funroll-loops`. By specifying the appropriate compiler and flags for MIPS
289 architecture, the configure tool will provide necessary settings to compile WRF.
290 Correspondingly, when compiling WRF on the benchmark platform, the compilation
291 flags are strictly consistent with those of MIPS CPU platform, which ensures that
292 differences in simulation results of two platforms are primarily attributed to the
293 underlying hardware architecture rather than changes in compilation settings.

294 In the CAMx model, the makefile provides information about parallelism and
295 compilers. Similarly, information about the CPU architecture, GNU compiler, and
296 compilation flags on MIPS platform also needs to be added in the makefile. For the
297 detailed information added in the makefile, please refer to Table 5. So far, the WRF-
298 CAMx model has been successfully compiled and installed on the MIPS platform after
299 modifications of the configuration files mentioned above.

300

301 **4 The differences of model results on the two platforms**

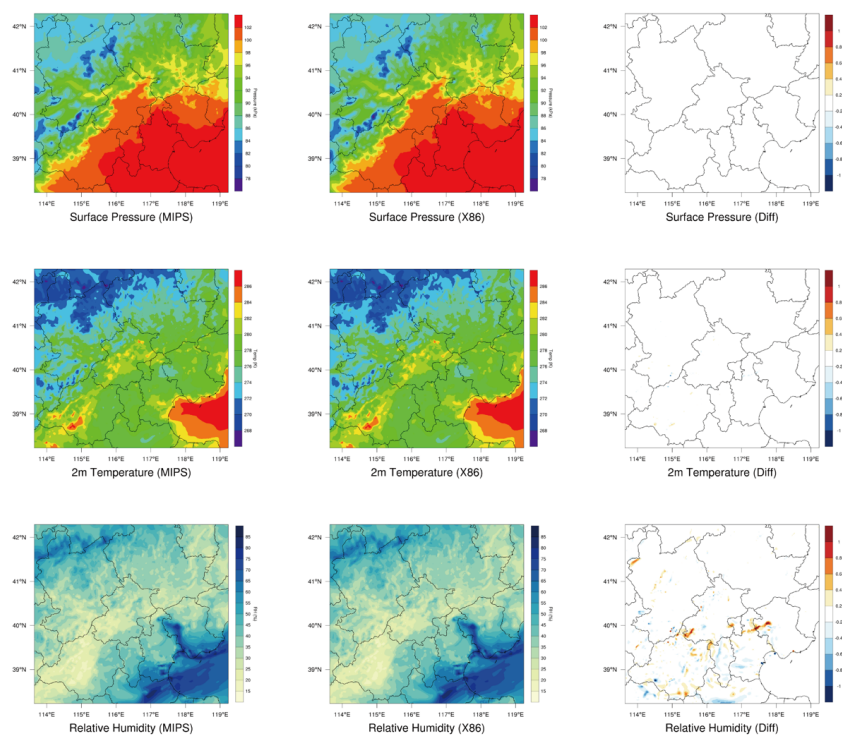
302 **4.1 Validation of the spatial distribution**

303 A simulation case has been designed to test the stability and availability of the
304 WRF-CAMx modeling system on the MIPS CPU platform in Beijing. Starting from
305 00:00 on November 3, 2020, until 24:00 on November 5, 2020, the modelling system
306 simulated the meteorological and air quality for a period of 72 hours, represents a
307 moderate-sized real scientific workload, which allows for testing in a short time, and
308 validating the results of the WRF-CAMx model on the MIPS platform and assessing



309 computational efficiency. By analyzing the differences in simulation results and
310 computing time, the accuracy and performance of the modeling system on MIPS
311 platform were evaluated, which further verifies the feasibility and stability of the
312 modeling system after porting to the MIPS platform.

313 Common meteorological variables, including 2-meter temperature, land surface
314 pressure, and relative humidity were selected to verify the WRF model results. Figure
315 3 shows the spatial distribution of the four meteorological variables after 72 hours
316 simulation on different platforms, as well as the absolute errors (AEs). The
317 meteorological variables from the modeling system on the different platforms exhibit a
318 generally consistent spatial distribution in the Beijing-Tianjin-Hebei regions shown in
319 Figure 3.



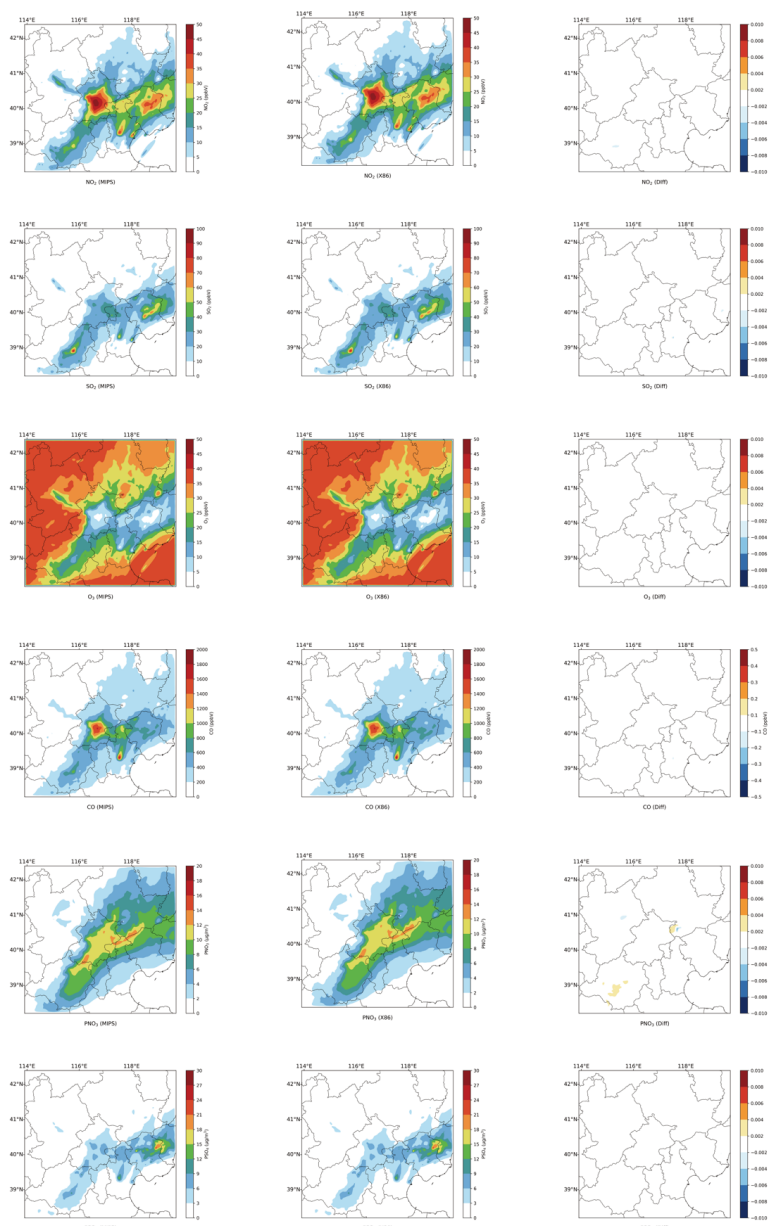
320
321 **Figure 3.** Spatial distribution of 2m temperature, surface pressure, relative humidity
322 from WRF. Left column, MIPS platform. Middle, the X86 platform. Right, the
323 differences between the MIPS and benchmark(X86) platform. Relative humidity is



324 calculated using the wrf-python package (Official website: [https://wrf-](https://wrf-python.readthedocs.io)
325 [python.readthedocs.io](https://wrf-python.readthedocs.io), last access: October 2023).

326

327 Similarly, the NO₂, SO₂, O₃, CO, PNO₃ and PSO₄ were selected to verify the
328 CAMx model results on the MIPS platform. Figure 4 shows the spatial distribution of
329 the six species, as well as the absolute errors (AEs) between the two platforms after 72
330 hours simulation. Simulating the 72h-case with four parallel processes using MPICH,
331 CAMx takes about 9h on Loongson 3A4000 CPU and 2.6h on Intel Xeon E5-2697 v4
332 CPU. As shown in Figure 4, the spatial distribution of air pollution concentrations from
333 the different platforms is essentially consistent, appearing very similar visually.



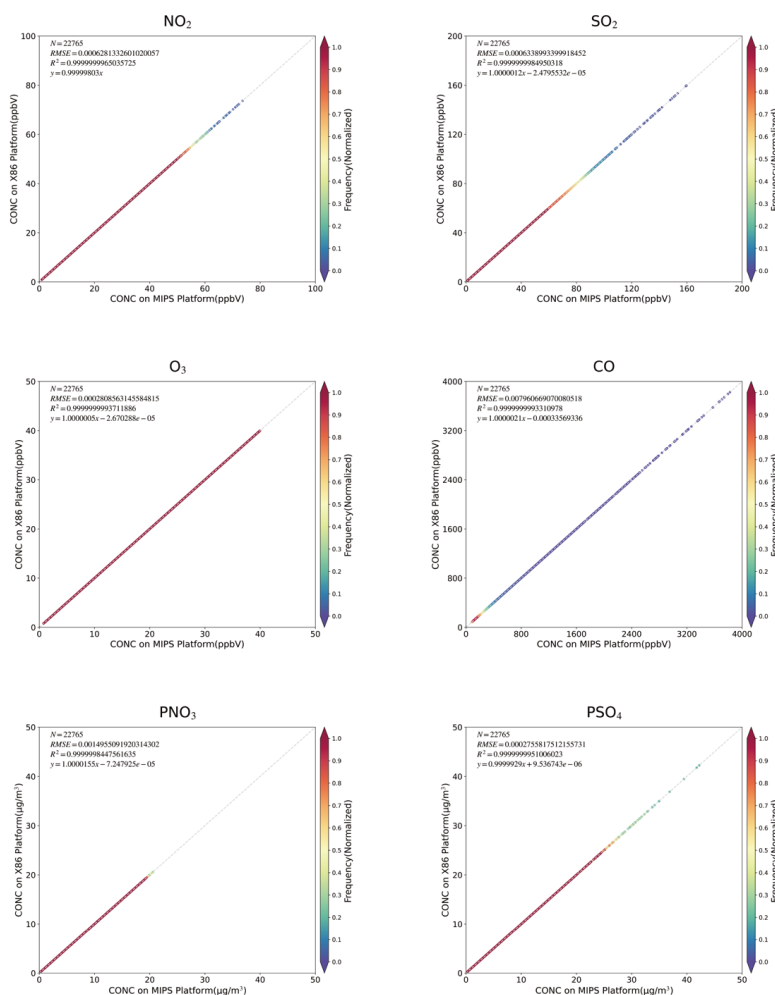
334

335 **Figure 4.** Spatial distribution of NO₂, SO₂, O₃, CO, PNO₃ and PSO₄ from CAMx on
336 MIPS and benchmark platform. Left column, MIPS platform. Middle, the X86 platform.
337 Right, the differences between the MIPS and benchmark(X86) platform.

338 As shown in Figure 5, the scatter plots between the two platform, it can be seen



339 that for the total of 22,765 grids within the 145x157 simulation domain, the root mean
 340 square errors (RMSEs) of the six species between the MIPS platform and benchmark
 341 platform are close to 0.001, which is essentially 0. The linear regression model was
 342 used to fit the scatters, and the regression slopes for each species are nearly 1, with
 343 intercepts close to 0, and the R2 values used for the goodness of fit are nearly 1. The
 344 fitted lines closely coincide with the “y=x” line, indicating that the differences between
 345 the MIPS and X86 platform for each species are minimal to negligible.

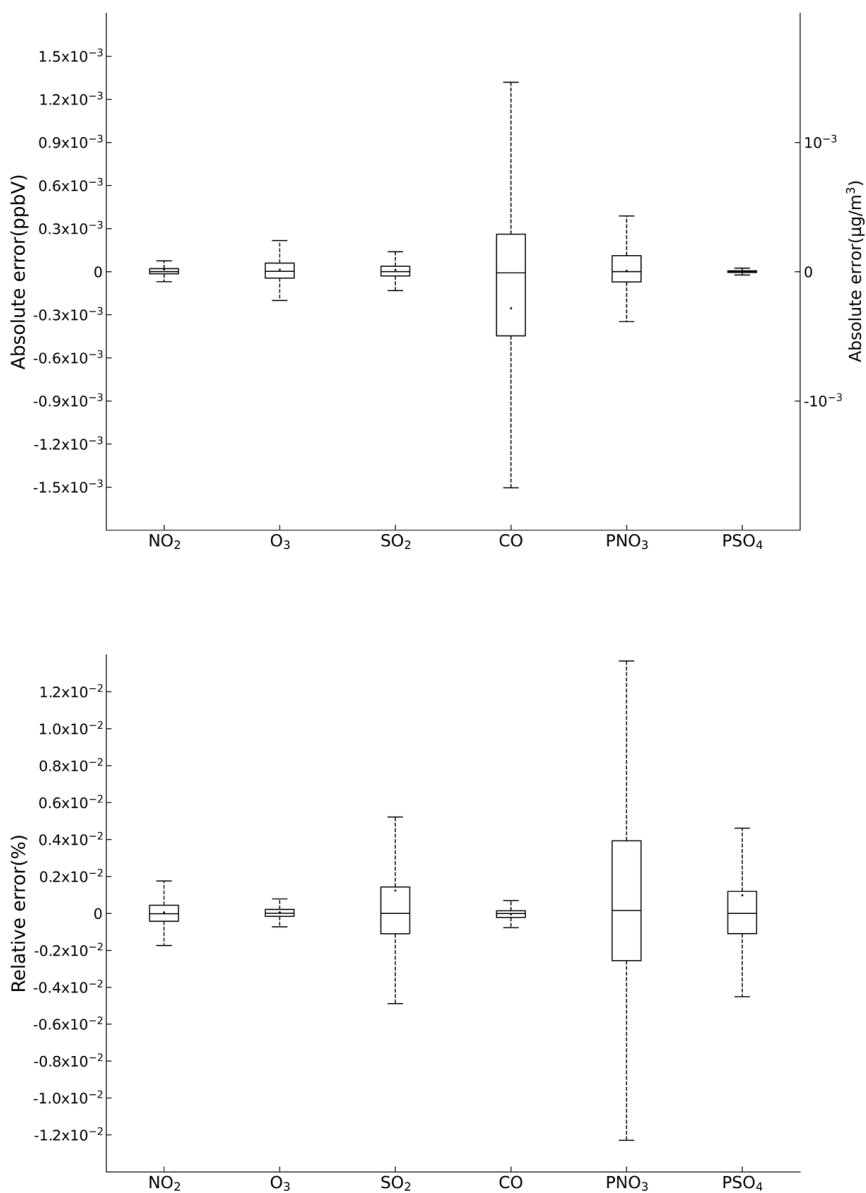


346
 347 **Figure 5.** Scatter of grid concentrations for NO₂, SO₂, O₃, CO, PNO₃ and PSO₄ from
 348 CAMx on the MIPS and benchmark platform. The density of scatters is represented by



349 the colors.

350 Figure 6 is the boxplots which show the absolute errors (AE) and relative errors
351 (RE) of the six species between MIPS and benchmark platform. According to Figure 6,
352 the absolute errors of the six species are generally in the range of $\pm 10^{-3}$ ppbv (parts per
353 billion by volume; the unit of NO₂, SO₂, O₃ and CO concentration) or $\mu\text{g m}^{-3}$ (the unit
354 of particle composition PNO₃ and PSO₄), and the relative errors are generally in the
355 range of $\pm 0.01\%$. Specially for CO, it exhibits more pronounced AEs compared to other
356 species. In some grid boxes, the AEs between MIPS and benchmark platform exceed
357 the range of $\pm 10^{-3}$ ppbv, but they remain in the range of $\pm 10^{-2}$ ppbv. In summary, there
358 are some errors between the results of the modeling system on the MIPS and benchmark
359 platform during the porting process. However, these errors are relatively minor
360 compared to the numerical values. The reasons are attributed to the differences in the
361 CPU architecture and compiler characteristics between the two platforms, such as data
362 operations and precision running on different CPUs, which are primarily responsible
363 for the observed errors.



364

365 **Figure 6.** The absolute errors and relative errors for NO₂, SO₂, O₃, CO, PNO₃ and PSO₄
366 concentration in all grids between the MIPS and benchmark platform.

367 Additionally, random grids in the domain were selected to assess the precision of
368 simulation results in localized regions. The positions of these grids were determined

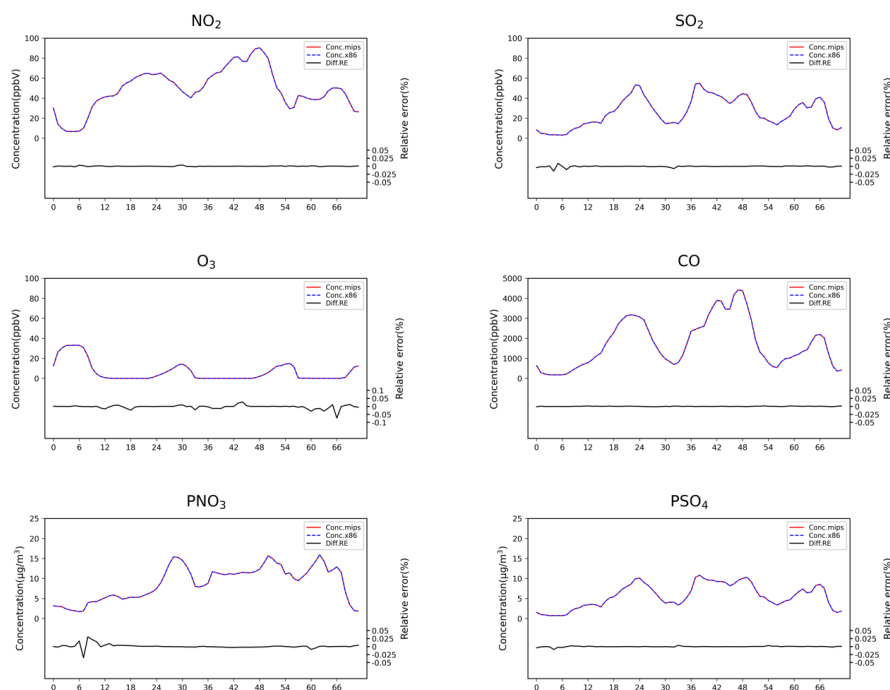


369 based on 32 observation stations in Beijing, and the nearest grid was determined using
370 the Euclidean Shortest Distance in the domain. The station map is presented in Figure
371 S1 in the Supplement. The Taylor diagram is used to assess the precision of
372 concentrations for six species near the observation stations, and the scatters
373 representing the six species at 32 stations are highly overlapping. Statistical parameters
374 used in the Taylor diagram, such as the correlation coefficient (R) approaching 1,
375 normalized standard deviation (NSD) and normalized root mean square error (NRMSE)
376 approaching 0, indicate high precision of the simulation results at specific stations on
377 the MIPS platform.

378

379 **4.2 Validation of the temporal distribution from the two platform**

380 The time series of computational differences also be evaluated in this study.
381 Random grid in the domain was selected to examine the hourly concentrations of the
382 six species. Taking the example of the Beijing Olympic Center station (116.40 E, 39.99
383 N) from the National Standard Air Quality (NSAQ) stations, the time series of hourly
384 concentrations in the grid of the Beijing Olympic Center station and relative errors
385 between the MIPS and benchmark platform over the 72-hour period were shown in
386 Figure 7. As shown in Figure 7, it can be seen that the time series of the air pollutant
387 concentrations were highly consistent between the two platforms. In the 72-hour period,
388 the relative errors for NO₂, SO₂, CO and PSO₄ remain in $\pm 0.025\%$. For PNO₃, the
389 relative errors remain in $\pm 0.05\%$, and for O₃, they remain in $\pm 0.1\%$. This indicates that
390 the errors caused by different architectures are within a reasonable range.



391

392 **Figure 7.** Time-series of NO₂, SO₂, O₃, CO, PNO₃ and PSO₄ concentrations and its
 393 relative errors (RE) at the Beijing Olympic Sports Center site between the MIPS and
 394 X86 platform. The red solid line and the blue dashed line, the CAMx model results on
 395 MIPS platform and X86 platform. The black solid line shows the relative errors (RE)
 396 between the MIPS and X86 platform.

397

398 To quantify the differences in the model results between the MIPS and benchmark
 399 platform, three statistical indicators are used to analyze the differences of concentration
 400 time series: Mean Absolute Error (MAE), Root Mean Square Error (RMSE), and Mean
 401 Absolute Percentage Error (MAPE). The MAPE quantifies the deviation between
 402 computational differences and simulated values. The smaller these indicators, the better
 403 accuracy and stability of scientific computing of the modeling system on the MIPS
 404 platform. The calculation formulas for these statistical indicators are provided in
 405 equations (1) to (3).

406
$$MAE = \frac{1}{n} \sum_{i=1}^n |MIPS(i) - Base(i)| \quad (1)$$

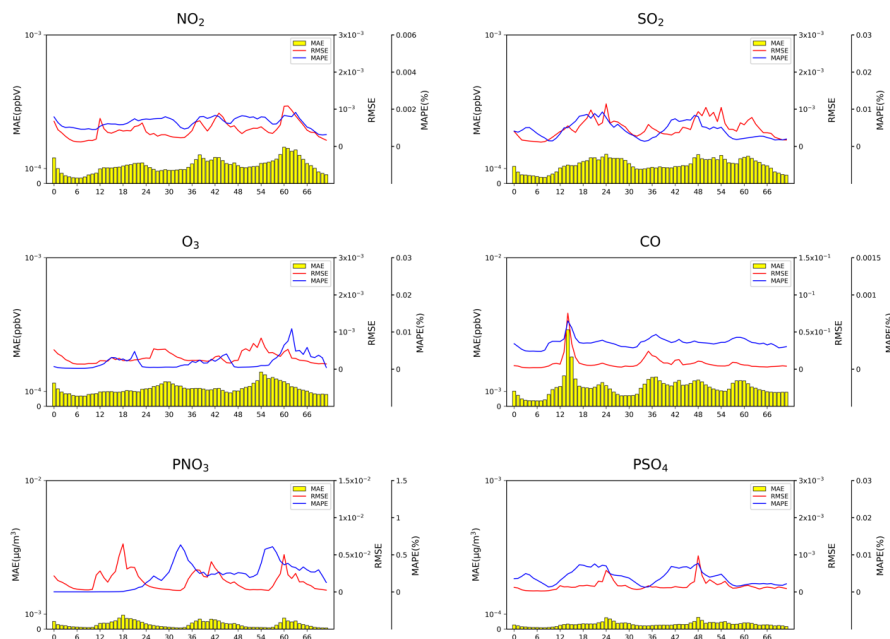


407
$$RMSE = \left[\frac{1}{n} \sum_{i=1}^n (MIPS(i) - Base(i))^2 \right]^{\frac{1}{2}} \quad (2)$$

408
$$MAPE = \frac{1}{n} \sum_{i=1}^n \left| \frac{MIPS(i) - Base(i)}{MIPS(i)} \right| \times 100\% \quad (3)$$

409 In the equations, n represents the number of grids in the domain. $MIPS(i)$ represents the
 410 simulated value of a certain grid on the MIPS platform, and $Base(i)$ represents the
 411 baseline value of a certain grid on the benchmark platform.

412 Figure 8 shows the time series of the concentration and their statistical indicators,
 413 MAE, RMSE, and MAPE during the 72-hour simulation. As show in the figure, for
 414 NO_2 , SO_2 , O_3 , and PSO_4 , the MAEs are all below 10^{-3} ppbv ($\mu\text{g m}^{-3}$), and the RMSEs
 415 are all below 10^{-3} . The MAEs for CO and PNO_3 are below 10^{-2} ppbv ($\mu\text{g m}^{-3}$), and the
 416 RMSEs for PNO_3 are below 10^{-2} , while the RMSEs for CO are below 10^{-1} . This is
 417 because that PNO_3 and CO have relatively higher background concentrations compared
 418 to the other species. The MAPE of PNO_3 concentration mainly ranging in 0-0.5%, while
 419 the MAPE of CO concentration has the lowest values below 0.001%, and the other
 420 species are in the range of 0-0.01%. Overall, the above time-series analysis verifies the
 421 accuracy and stability of the modeling system on the MIPS platform.



422

423 **Figure 8.** Time series of MAEs, RMSEs and MAPEs for NO_2 , SO_2 , O_3 , CO, PNO_3 and



424 PSO_4 concentration in the 72h simulation. The yellow bar, the MAE. The red lines,
425 RMSE, the blue lines, MAPE.

426

427 In this study, the evaluation method proposed by Wang et al. (2021) was also used
428 to assess the scientific applicability of the model results on the MIPS platform. The
429 RMSEs for NO_2 , SO_2 , O_3 , CO , PNO_3 and PSO_4 concentration between the MIPS and
430 benchmark platform were computed, along with the standard deviation used to describe
431 the spatial variation of species, and the ratio of RMSE to std, as shown in Table 6. The
432 differences of the four species between the two platforms are negligible compared to
433 their own spatial variations. Therefore, the results on the MIPS platform meet the
434 accuracy requirements for research purpose.

435

436 **Table 6.** RMSE, std, RMSE/std for NO_2 , SO_2 , O_3 , CO , PNO_3 and PSO_4 .

	Differences in results	Spatial variation	RMSE/std
	RMSE	std	
NO_2	6.3×10^{-7}	0.01	5.9×10^{-5}
O_3	2.8×10^{-7}	0.01	2.5×10^{-5}
SO_2	6.3×10^{-7}	0.02	3.9×10^{-5}
CO	7.9×10^{-6}	0.30	2.6×10^{-5}
PNO_3	1.5×10^{-3}	3.8	3.9×10^{-4}
PSO_4	2.7×10^{-4}	3.9	6.9×10^{-5}

437

438 In fact, the differences in model results cannot be completely eliminated, primarily
439 due to the varying CPU architectures and compilers. In the practical applications,
440 compared with the errors arising from the inherent uncertainties of the modeling system
441 and the input data, the differences of model results between different platforms can even
442 be considered negligible. The comprehensive analysis demonstrates that the results of
443 the WRF-CAMx modeling system on the MIPS CPU platform are reasonable.

444

445 **5 The evaluation about computational performance**

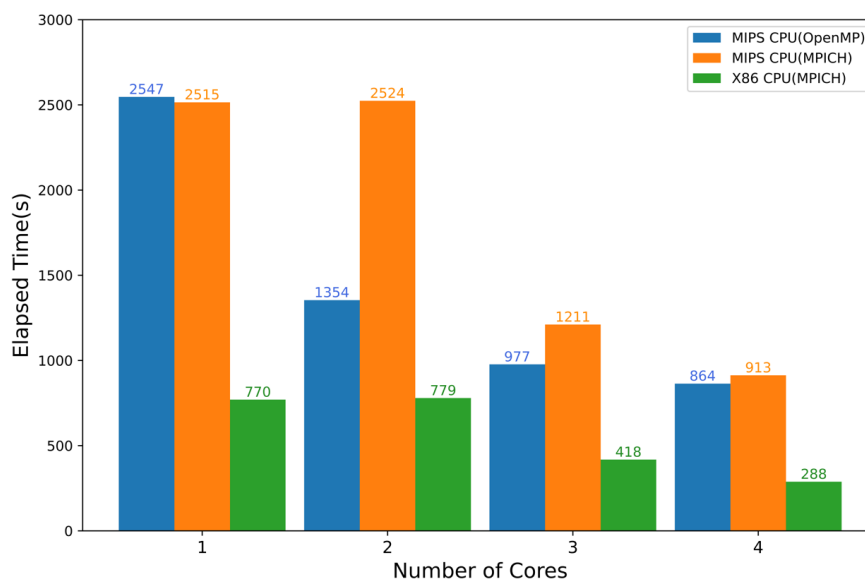
446 Scientific computing involves a significant amount of floating-point operations,
447 and the floating-point computational capability is a crucial indicator for CPU



448 performance. In this study, the simulation case was configured to conduct parallel
449 computing tests on the MIPS and benchmark platform. These tests included assessing
450 the CPU's single-core performance with the non-parallel model and the platform's
451 parallel performance with the parallel model using multiple processes. The time of
452 CAMx model running simulation case for 2 hours in the modeling system are shown in
453 Figure 9. From the figure, it can be observed that under single-core conditions, the
454 computing capability of the MIPS platform for CAMx is approximately one-third of
455 the X86 benchmark platform.

456 It's worth noting that the simulation time of the CAMx model for running with two
457 processes in parallel and running in non-parallel remains approximately consistent.
458 This is because the MPI used in CAMx is designed using a "master/slave" parallel
459 processing approach, and a process is allocated for input/output and message
460 communication during the runtime (Cao K et al., 2023). This process doesn't perform
461 any simulation in the model. Therefore, the time required for parallelism of two
462 processes is comparable to the non-parallelism, and in some cases, it might even be
463 slightly longer due to the overhead of MPI communication. Compared to non-parallel,
464 the speedup of the MIPS platform with four-process parallelism using MPICH3 is
465 approximately 2.8, while using OpenMP is about 2.9. For the X86 benchmark platform,
466 running with four processes in parallel using MPICH3 has a speedup of approximately
467 2.7.

468 Additionally, the performance of the MIPS platform significantly decreases when
469 the number of parallel processes exceeds 4. This is because the modeling system
470 involves compute-intensive tasks. The Loongson 3A4000 CPU has four cores, and
471 when the number of processes called by MPI matches the number of CPU cores, the
472 CPU utilization can approach 100%. Further increasing the number of processes, the
473 cores will compete for CPU resources, resulting in additional overhead and reduced
474 computational efficiency.



475

476 **Figure 9.** Elapsed time of CAMx model running simulation case for 2 hours on the
477 MIPS and benchmark platforms.

478

479 In the recent years, the Longsoon CPUs have been continuously upgraded.
480 Compared to the previous generations of products, the performance of the Longsoon
481 3A4000 CPU has shown significant improvement. Wu et al. (2019) simulated a nested
482 domain covering Beijing for 48 hours using the MM5 model on the Longsoon 3A quad-
483 core CPU platform. The results showed that the computational capacity of the
484 Longsoon 3A platform for the MM5 model is approximately equivalent to around 1/12
485 of the Intel Core 2 Q8400 quad-core CPU, which was released in the same year. In the
486 study of Luo et al. (2011), a comparison between Loongson 3A and Intel i5 was made
487 by running NPB benchmark on each platform. The results shows that the performance
488 of the 3A is nearly one-tenth of that of the i5. The rapid development of Loongson
489 CPUs has provided a strong hardware foundation for the application of numerical
490 simulation and scientific computing on MIPS architecture CPU platforms. The
491 adaptation and optimization of the models based on MIPS CPUs will also be an
492 important research direction in the future.

493



494 **6 Conclusion**

495 This study describes the application of the WRF-CAMx model on the MIPS CPU
496 platform. The platform used in this study is Loongson 3A4000 quad-core 2.0GHz CPU,
497 offering a peak operational speed of 128GFlops. It is equipped with the MIPS GNU
498 compiler. The benchmark platform used the Intel Xeon E5-2697 v4 CPU along with the
499 same version of X86 GNU compiler. Based on the characteristics of CPU architecture
500 and compiler, this study has successfully completed the construction of runtime
501 environment for the WRF-CAMx modeling system. The application of an air quality
502 modelling system based on WRF-CAMx was successfully tested using a 72-hour
503 simulation case in the Beijing-Tianjin-Hebei region.

504 The results showed that the spatial distribution of the meteorological variables and
505 air pollutant species was nearly identical, with relative errors in the range of $\pm 0.1\%$.
506 Statistically, the maximum MAEs of major species ranged from 10^{-3} to 10^{-2} ppbv ($\mu\text{g m}^{-3}$),
507 the maximum RMSEs ranged from 10^{-2} to 10^{-1} ppbv ($\mu\text{g m}^{-3}$), and the MAPEs
508 remained within 0.5%, that the differences caused by the architectures and compilers
509 were within a reasonable range. Simulating a 2h-case with four parallel processes using
510 MPICH, CAMx takes about 15.2min on Loongson 3A4000 CPU and 4.8 min on Intel
511 Xeon E5-2697 v4 CPU. In terms of single-core CPU performance, the single-core
512 computing capability of Loongson 3A4000 CPU for the WRF-CAMx modeling system
513 is about one-third of Intel Xeon E5-2697 v4 CPU.

514 Currently, Loongson Technology has introduced the LoongArch architecture
515 which is compatible with MIPS, and it has been used in the next-generation product,
516 the 3A5000 CPU (Hu et al., 2022). It is foreseeable that the LoongArch architecture
517 will lead to more significant performance improvements. In the future, as the numerical
518 models become more complex and computational scales become larger, more models
519 will be tested on high-performance computing platforms equipped with the LoongArch
520 architecture CPUs.

521

522 **Code and data availability.** The source codes of CAMx version 6.10 are available at



523 <https://camx-wp.azurewebsites.net/download/source> (ENVIRON, 2023). The datasets
524 related to this paper and the CAMx codes for MIPS CPU are available online via
525 ZENODO (<https://zenodo.org/records/10297970>).

526

527 **Supplement.** The supplement related to this article is available on-line.

528

529 **Author contributions.** ZB and QW conducted the simulation and prepared the materials.
530 QW planned and organized the project. ZB and QW completed the porting and
531 application of the model for MIPS CPU. YS collected and prepared the emission data
532 for the simulation. ZB, QW, KC, and HC participated in the discussion.

533

534 **Acknowledgements.** The National Key R&D Program of China (2020YFA0607804)
535 and the Beijing Advanced Innovation Program for Land Surface funded this work. The
536 research is supported by the High Performance Scientific Computing Center (HSCC)
537 of Beijing Normal University.

538

539 **Competing interests.** The contact author has declared that none of the authors has any
540 competing interests.

541

542 **References**

- 543 Amer, A., Balaji, P., Bland, W., Gropp, W., Guo, Y., Latham, R., Lu, H., Oden, L., Pena, A. J.,
544 Raffenetti, K., Seo, S., Si, M., Thakur, R., Zhang, J., and Zhao, X.: MPICH User's Guide
545 Version 3.4, available at: <https://www.mpich.org/static/downloads/3.4/mpich-3.4-userguide.pdf> ,
546 2021.
- 547 Appel, K. W., Napelenok, S. L., Foley, K. M., Pye, H. O. T., Hogrefe, C., Luecken, D. J., Bash, J.
548 O., Roselle, S. J., Pleim, J. E., Foroutan, H., Hutzell, W. T., Pouliot, G. A., Sarwar, G., Fahey, K.
549 M., Gantt, B., Gilliam, R. C., Heath, N. K., Kang, D., Mathur, R., and Schwede, D. B.: Description
550 and evaluation of the Community Multiscale Air Quality (CMAQ) modeling system version 5.1,
551 Geoscientific Model Development, 10, 1703–1732, <https://doi.org/10.5194/gmd-10-1703-2017>,
552 2017.
- 553 Appel, K. W., Bash, J. O., Fahey, K. M., Foley, K. M., Gilliam, R. C., Hogrefe, C., Hutzell, W. T.,
554 Kang, D., Mathur, R., Murphy, B. N., Napelenok, S. L., Nolte, C. G., Pleim, J. E., Pouliot, G. A.,
555 Pye, H. O. T., Ran, L., Roselle, S. J., Sarwar, G., Schwede, D. B., Sidi, F. I., Spero, T. L., and
556 Wong, D. C.: The Community Multiscale Air Quality (CMAQ) model versions 5.3 and 5.3.1:



- 557 system updates and evaluation, *Geoscientific Model Development*, 14, 2867–2897,
558 <https://doi.org/10.5194/gmd-14-2867-2021>, 2021.
- 559 Bai, X., Tian, H., Liu, X., Wu, B., Liu, S., Hao, Y., Luo, L., Liu, W., Zhao, S., Lin, S., Hao, J., Guo,
560 Z., and Lv, Y.: Spatial-temporal variation characteristics of air pollution and apportionment of
561 contributions by different sources in Shanxi province of China, *Atmospheric Environment*, 244,
562 117926, <https://doi.org/10.1016/j.atmosenv.2020.117926>, 2021.
- 563 Cao, K., Wu, Q., Wang, L., Wang, N., Cheng, H., Tang, X., Li, D., and Wang, L.: GPU-HADVPPM
564 V1.0: a high-efficiency parallel GPU design of the piecewise parabolic method (PPM) for
565 horizontal advection in an air quality model (CAMx V6.10), *Geosci. Model Dev.*, 16, 4367–4383,
566 <https://doi.org/10.5194/gmd-16-4367-2023>, 2023.
- 567 Chen, H. S., Wang, Z. F., Li, J., Tang, X., Ge, B. Z., Wu, X. L., Wild, O., and Carmichael, G. R.:
568 GNAQPMS-Hg v1.0, a global nested atmospheric mercury transport model: model description,
569 evaluation and application to trans-boundary transport of Chinese anthropogenic emissions,
570 *Geoscientific Model Development*, 8, 2857–2876, <https://doi.org/10.5194/gmd-8-2857-2015>,
571 2015.
- 572 George, A. D.: An overview of RISC vs. CISC, in: [1990] Proceedings. The Twenty-Second
573 Southeastern Symposium on System Theory, The Twenty-Second Southeastern Symposium on
574 System Theory, Cookeville, TN, USA, 436–438, <https://doi.org/10.1109/SSST.1990.138185>,
575 1990.
- 576 Guo, L. and Liu, Y.: Efficient Implementation of FFT on Loongson 3A CPU, *Journal of Chinese*
577 *Computer Systems*, 33, 594–597, 2012 (in Chinese).
- 578 Hennessy, J., Jouppi, N., Przybylski, S., Rowen, C., Gross, T., Baskett, F., and Gill, J.: MIPS: A
579 microprocessor architecture, *SIGMICRO Newsl.*, 13, 17–22,
580 <https://doi.org/10.1145/1014194.800930>, 1982.
- 581 Hu, W., Wang, J., Gao, X., Chen, Y., Liu, Q., and Li, G.: Godson-3: A Scalable Multicore RISC
582 Processor with x86 Emulation, *IEEE Micro*, 29, 17–29, <https://doi.org/10.1109/MM.2009.30>,
583 2009.
- 584 Hu, W., Zhang, Y., and Fu, J.: An introduction to CPU and DSP design in China, *Sci. China Inf. Sci.*,
585 59, 1–8, <https://doi.org/10.1007/s11432-015-5431-6>, 2016.
- 586 Hu, W., Gao, X., and Zhang, G.: Building the software ecosystem for the Loongson instruction set
587 architecture, *Information and Communications Technology and Policy*, 43–48, 2022 (in Chinese).
- 588 Hu, W.-W., Gao, Y.-P., Chen, T.-S., and Xiao, J.-H.: The Godson Processors: Its Research,
589 Development, and Contributions, *J. Comput. Sci. Technol.*, 26, 363–372,
590 <https://doi.org/10.1007/s11390-011-1139-2>, 2011.
- 591 Intel Inc.: Intel® 64 and IA-32 Architectures Software Developer’s Manual, Volume 1: Ba
592 sic Architecture, available at: [https://www.intel.com/content/www/us/en/developer/articles/te
593 chnical/intel-sdm.html](https://www.intel.com/content/www/us/en/developer/articles/technical/intel-sdm.html), 2023.
- 594 Li, L., Chen, Y.-J., Liu, D.-F., Qian, C., and Hu, W.-W.: An FFT Performance Model for Optimizing
595 General-Purpose Processor Architecture, *J. Comput. Sci. Technol.*, 26, 875–889,
596 <https://doi.org/10.1007/s11390-011-0186-z>, 2011.
- 597 Li, L., Chen, Z., and Wang, S.: Power Consumption and Analysis of Server Based on Loongson
598 CPU No. 3, *Information Technology & Standardization*, 46–50, 2014 (in Chinese).
- 599 Liu, Y., Ye, K., and Xu, C.-Z.: Performance Evaluation of Various RISC Processor Systems: A Case
600 Study on ARM, MIPS and RISC-V, in: *Cloud Computing – CLOUD 2021*, Cham, 61–74,



- 601 https://doi.org/10.1007/978-3-030-96326-2_5, 2022.
- 602 Luo, Q., Kong, C., Cai, Y., and Liu, G.: Performance Evaluation of OpenMP Constructs and Kernel
603 Benchmarks on a Loongson-3A Quad-Core SMP System, in: 2011 12th International Conference
604 on Parallel and Distributed Computing, Applications and Technologies, 2011 12th International
605 Conference on Parallel and Distributed Computing, Applications and Technologies, 191–196,
606 <https://doi.org/10.1109/PDCAT.2011.66>, 2011.
- 607 Mallach, E. G.: RISC: Evaluation and Selection, *Journal of Information Systems Management*, 8,
608 8–16, <https://doi.org/10.1080/07399019108964978>, 1991.
- 609 Michalakes, J., Chen, S., Dudhia, J., Hart, L., Klemp, J., Middlecoff, J., and Skamarock, W.:
610 Development of a next-generation regional weather research and forecast model, in:
611 Developments in Teracomputing, WORLD SCIENTIFIC, 269–276,
612 https://doi.org/10.1142/9789812799685_0024, 2001.
- 613 MIPS Technology Inc.: MIPS Architecture For Programmers Volume I-A, available at:
614 <https://www.mips.com/products/architectures/mips64>, 2014.
- 615 Pepe, N., Pirovano, G., Lonati, G., Balzarini, A., Toppetti, A., Riva, G. M., and Bedogni, M.:
616 Development and application of a high resolution hybrid modelling system for the evaluation of
617 urban air quality, *Atmospheric Environment*, 141, 297–311,
618 <https://doi.org/10.1016/j.atmosenv.2016.06.071>, 2016.
- 619 RAMBOLL ENVIRON Inc.: CAMx User’s Guide Version 6.1, available at: [https://camx-
620 wp.azurewebsites.net/Files/CAMxUsersGuide_v6.10.pdf](https://camx-wp.azurewebsites.net/Files/CAMxUsersGuide_v6.10.pdf), 2014.
- 621 Shi, Z.: Technology comparison and research of RISC and CISC, *China Science and Technology
622 Information*, 131–132, 2008 (in Chinese).
- 623 Skamarock, C., Klemp, B., Dudhia, J., Gill, O., Liu, Z., Berner, J., Wang, W., Powers, G., Duda, G.,
624 Barker, D., and Huang, X.: A Description of the Advanced Research WRF Model Version 4,
625 <https://doi.org/10.5065/1dfh-6p97>, 2019.
- 626 Sun Y.: Research on the contribution of soil fugitive dust in Beijing based on satellite identification
627 and numerical simulation technology, Master, Beijing Normal University, <https://etdlib.bnu.edu.cn>,
628 2022a.
- 629 Sun, Y., Wu, Q., Wang, L., Zhang, B., Yan, P., Wang, L., Cheng, H., Lv, M., Wang, N., and Ma, S.:
630 Weather Reduced the Annual Heavy Pollution Days after 2016 in Beijing, *Sola*, 18, 135–139,
631 <https://doi.org/10.2151/sola.2022-022>, 2022b.
- 632 The HDF Group: HDF5 User’s Guide Version 1.1, available at:
633 <https://portal.hdfgroup.org/display/HDF5/HDF5+User+Guides>, 2019.
- 634 UCAR/Unidata: NetCDF User’s Guide Version 1.1, available at: <https://docs.unidata.ucar.edu/nug> ,
635 2021.
- 636 Wang, K., Gao, C., Wu, K., Liu, K., Wang, H., Dan, M., Ji, X., and Tong, Q.: ISAT v2.0: an
637 integrated tool for nested-domain configurations and model-ready emission inventories for WRF-
638 AQM, *Geoscientific Model Development*, 16, 1961–1973, [https://doi.org/10.5194/gmd-16-1961-
639 2023](https://doi.org/10.5194/gmd-16-1961-2023), 2023.
- 640 Wang, P., Jiang, J., Lin, P., Ding, M., Wei, J., Zhang, F., Zhao, L., Li, Y., Yu, Z., Zheng, W., Yu, Y.,
641 Chi, X., and Liu, H.: The GPU version of LASG/IAP Climate System Ocean Model version 3
642 (LICOM3) under the heterogeneous-compute interface for portability (HIP) framework and its
643 large-scale application, *Geosci. Model Dev.*, 14, 2781–2799, [https://doi.org/10.5194/gmd-14-
644 2781-2021](https://doi.org/10.5194/gmd-14-2781-2021), 2021.



- 645 Wang, S., Li, L., and Chen, Z.: The Test and Analysis on Memory Access Performance Based on
646 Loongson CPU, *Information Technology & Standardization*, 32–36, 2014 (in Chinese).
- 647 Wang, Z., Xie, F., Wang, X., An, J., and Zhu, J.: Development and Application of Nested Air Quality
648 Prediction Modeling System, *Chinese Journal of Atmospheric Sciences*, 778–790,
649 <http://dx.doi.org/10.3878/j.issn.1006-9895.2006.05.07>, 2006.
- 650 Wu, Q. and Cheng, H.: Transplantation and application of mesoscale mode on Loongson CPU
651 platform, *Journal of Beijing Normal University (Natural Science)*, 55, 11–18,
652 <https://doi.org/10.16360/j.cnki.jbnuns.2019.01.002>, 2019.
- 653 Wu, Q., Xu, W., Shi, A., Li, Y., Zhao, X., Wang, Z., Li, J., and Wang, L.: Air quality forecast of
654 PM10 in Beijing with Community Multi-scale Air Quality Modeling (CMAQ) system: emission
655 and improvement, *Geoscientific Model Development*, 7, 2243–2259,
656 <https://doi.org/10.5194/gmd-7-2243-2014>, 2014.
- 657 Wu, Y., Xu, G., Zhao, Y., and Tan, Y.: Parallel Processing on WRF Meteorological Data Using
658 MPICH, in: 2012 Sixth International Conference on Internet Computing for Science and
659 Engineering, 2012 Sixth International Conference on Internet Computing for Science and
660 Engineering, titleTranslation:, 262–265, <https://doi.org/10.1109/ICICSE.2012.12>, 2012.
- 661 Xiao, H., Wu, Q., Yang, X., Wang, L., and Cheng, H.: Numerical study of the effects of initial
662 conditions and emissions on PM2.5 concentration simulations with CAMx v6.1: a Xi'an case
663 study, *Geoscientific Model Development*, 14, 223–238, [https://doi.org/10.5194/gmd-14-223-](https://doi.org/10.5194/gmd-14-223-2021)
664 [2021](https://doi.org/10.5194/gmd-14-223-2021), 2021.
- 665 Yang, X., Xiao, H., Wu, Q., Wang, L., Guo, Q., Cheng, H., Wang, R., and Tang, Z.: Numerical study
666 of air pollution over a typical basin topography: Source appointment of fine particulate matter
667 during one severe haze in the megacity Xi'an, *Science of The Total Environment*, 708, 135213,
668 <https://doi.org/10.1016/j.scitotenv.2019.135213>, 2020.
- 669 Zhang, Y., Bocquet, M., Mallet, V., Seigneur, C., and Baklanov, A.: Real-time air quality forecasting,
670 part I: History, techniques, and current status, *Atmospheric Environment*, 60, 632–655,
671 <https://doi.org/10.1016/j.atmosenv.2012.06.031>, 2012.
- 672 Zhang, Z., Wang, X., Cheng, S., Guan, P., Zhang, H., Shan, C., and Fu, Y.: Investigation on the
673 difference of PM2.5 transport flux between the North China Plain and the Sichuan Basin,
674 *Atmospheric Environment*, 271, 118922, <https://doi.org/10.1016/j.atmosenv.2021.118922>, 2022.
- 675 Zhao, M., Zhang, Y., Liu, Y., Li, Y., and Yan, S.: Comparison and Analysis of Three Types of FFT
676 Adaptive Libraries on Loongson 3A, *Computer Science*, 39, 281–285, 2012 (in Chinese).
- 677 Zhen, J., Guan, P., Yang, R., and Zhai, M.: Transport matrix of PM2.5 in Beijing-Tianjin-Hebei and
678 Yangtze River Delta regions: Assessing the contributions from emission reduction and
679 meteorological conditions, *Atmospheric Environment*, 304, 119775,
680 <https://doi.org/10.1016/j.atmosenv.2023.119775>, 2023.
- 681 Zhi, Y. and Xu, J.: Android transplantation and analysis based on Loongson, in: 2012 International
682 Conference on Information Management, Innovation Management and Industrial Engineering,
683 2012 International Conference on Information Management, Innovation Management and
684 Industrial Engineering, 59–61, <https://doi.org/10.1109/ICIII.2012.6339777>, 2012.